CCFE
CULHAM CENTRE FOR FUSION ENERGY

UK Atomic Energy Authority

UKAEA-CCFE-PR(21)12

M. Richardson, M. Gorley, Y. Wang, D. Andres, H. Dawson

Small punch creep investigation of Eurofer97 and 14Cr Oxide Dispersion Strengthened Steel

Small punch creep investigation of Eurofer97 and 14Cr Oxide Dispersion Strengthened Steel

M. Richardson, M. Gorley, Y. Wang, D. Andres, H. Dawson

This is a preprint of a paper submitted for publication in
Journal of Nuclear Materials

Small punch creep investigation of Eurofer97 and 14Cr Oxide Dispersion Strengthened Steel

M. Richardson[a*], M. Gorley[a], Y. Wang[a], D. Andres[a], H. Dawson[a]

[a]UKAEA, Culham Science Centre, Abingdon, Oxfordshire, OX14 3DB, UK

*Corresponding Author: mark.richardson@ukaea.uk

Abstract

Small punch creep (SPC) testing represents an effective way to rapidly assess the creep performance of novel materials and potentially monitor degradation of in-service components. Recent progress in standardisation has also led to improvements in data analysis. However, estimation of equivalent uniaxial stresses is still somewhat challenging and has hindered wider usage of the small punch technique. In this study, the creep properties of two candidate materials for structural applications in future fusion reactors were assessed via SPC. These included the baseline structural material, Eurofer97, and a more recently developed 14Cr Oxide Dispersion Strengthened (ODS) steel (14YWT). Having been assessed at 550 °C, the 14YWT demonstrated superior creep life and significantly lower rates of deformation, but also exhibited reduced ductility. The Modified Chakrabarty (MCH) approach was employed to estimate equivalent uniaxial creep stresses. This methodology appeared to work well with the Eurofer97 but struggled when applied to 14YWT, making accurate estimation of the 14YWT performance difficult. Since the MCH approach was developed for ductile materials, its predictive capabilities may have been limited by the low ductility of 14YWT.

Key Words: Small Punch Creep, Eurofer97, ODS Steel, 14YWT, SSTT

1. Introduction

The prospect of delivering almost unlimited clean energy in a controlled manner makes nuclear fusion one of the most sought after goals in tackling climate change and the energy crisis [1]. However, the development of large scale fusion power plants represents one of the greatest engineering challenges facing humankind today [2]. The environment within a commercial fusion power plant reactor will be one of the most hostile imaginable, with materials exposed to high heat flux, neutron irradiation, plasma erosion, static and dynamic stresses, thermal cycling and many other demanding loads [1][2][3]. Development of structural materials capable of withstanding these conditions is a major objective of many fusion development programs worldwide [3].

For the EU DEMO, the current baseline structural material is the Reduced Activation Ferritic Martensitic (RAFM) steel Eurofer97 [4][5]. RAFM steels, such as Eurofer97 were chosen over austenitic stainless steels due to their superior swelling resistance under irradiation, higher thermal conductivity and lower thermal expansion [6]. However, despite the relative maturity of RAFMs, their operating temperature range is somewhat narrow, being constrained by radiation embrittlement at low temperature and creep performance at high temperature, giving a viable window of 325 – 550 °C [7]. For this reason, there have been ongoing attempts to develop superior alternatives to RAFM steels. One approach currently being explored is the use of nanoscale oxide particles to improve mechanical properties and radiation resistance. A key advantage of this strengthening mechanism is the thermal stability of the oxide particles, providing greater high temperature strength and creep performance [7][8][9]. While these Oxide Dispersion Strengthened (ODS) steels have shown significant promise, they are costly and time consuming to produce [7].

Separately, the development of high fluence neutron test facilities is underway to provide a more suitable environment in which to expose candidate materials e.g. the International Fusion Materials Irradiation Facility-DEMO Oriented Neutron Source (IFMIF-DONES) [4][10][11][12][13]. However, the high flux irradiation volume in current designs will be somewhat limited (≤500ml) [11][13][14][15]. Consequently, this has prompted significant interest in the use of subsize specimens and other small scale test techniques (SSTT) [13][16][17]. SSTT is also of interest to the fission industry, since surveillance specimens have long been used in operating reactors to monitor material degradation [18][19] and reducing the size of these is useful for both space, re-use (of larger tested specimens) and activation reasons [20].

The small punch test is one such SSTT that has the potential to assess mechanical performance using reduced volumes of material. It also has the potential to accelerate alloy development by allowing the rapid assessment of small batches of novel alloys [21]. Given the limited production volume of ODS steels, they are an ideal candidate for assessment via such small sample testing techniques (SSTT). Small punch involves forcing a hemispherical punch or ball through a disk-shaped specimen under constant load (Small Punch Creep, SPC) or constant displacement rate [22][21][23]. The latter provides force-displacement data, while SPC can produce displacement-time curves, an example of which can be seen in Figure 1. The standard dimensions for a small punch test specimen are a thickness of 0.5 mm and a dimeter of 8 mm [22][24]. Given the small volume of material required, the test can be considered pseudo non-destructive, with techniques available for the in-situ removal of material from large components [22].

However, determining the mechanical properties (such as tensile and creep) of materials via small punch testing is still challenging due to the complex stress state that occurs during deformation [23][25]. Materials can be ranked by their relative performance [21], but require consistency in test methodology and data analysis to ensure reliability. Ongoing attempts at standardisation are intended to help address this [26][27], which will be critical if regulators are to accept the validity of SSTT data [28]. This paper therefore utilises the recently developed 'Modified Chakrabarty' (MCH) approach for force-stress conversion [29] to assess the SPC performance of Eurofer97 and a prospective 14Cr ODS steel (14YWT).

2. Materials and Experimental Method

The Eurofer97 used in this study was supplied by the Karlsruhe Institute for Technology in the form of a 5 mm thick plate, produced by Bohler Bleche GMBH. After normalising at 980 °C, the plate was tempered at 760 °C for 90 minutes. The composition is detailed in Table 1. The ODS steel assessed was a 14Cr steel known as 14YWT [30]. The nominal composition (wt%) was 14Cr, 3W, 0.2Ti, $0.25Y_2O_3$. Fabrication was carried out using gas-atomised pre-alloyed powder (excluding Y_2O_3) supplied by Aubert & Duval. The oxide particles were introduced through the addition of Y_2O_3 during mechanical alloying (MA). This was performed using a Fritsch Pulverisette P5 planetary ball mill at 250 rpm for 60 hours under an argon environment. To address contamination issues, milling pots and balls were custom made from AISI 50-100. The milling balls were 10 mm in diameter and a ball-to-powder weight ratio of 10:1 was employed. Consolidation was achieved through Hot Isostatic Pressing (HIP), carried out at 1150 °C under 150 MPa of pressure for a duration of four hours [30]. Table 1 illustrates the composition of the resulting product.

Characterisation of the starting microstructures was carried out through Electron Backscatter Diffraction (EBSD) using a TESCAN Field Emission Gun Scanning Electron Microscope (FEG SEM) for

the Eurofer97 and a JOEL 6500F FEG SEM for the 14YWT. Due to the bimodal grain size of the 14YWT, multiple step sizes were used to characterise the microstructure at different length scales (0.1 µm and 0.65 µm for high and low magnification, respectively). The Eurofer97 could be adequately represented at an intermediate magnification with a step size of 0.11 µm. Post-processing of the Eurofer97 EBSD data was carried out using Oxford Instruments HKL CHANNEL5 software [31], while the 14YWT had previously been analysed using EDAX Inc, TSL OIM software [30]. The Vickers hardness was ascertained using a Leco LM 100AT microhardness tester, with a 500 g load and a dwell time of 13 s. A minimum of 40 indents were made across specimens to provide a reliable average.

Figure 1(a) illustrates the small punch setup employed in this study. Specimens 8 mm in diameter were removed from the as-received material through Electro-Discharge Machining (EDM), before wet grinding with SiC paper to reach their final thickness. The Eurofer97 specimens were oriented such that the flat face of each disk was parallel to the plane of the rolled plate (and therefore in the plane of the rolling direction). To remove the 14YWT specimens, a slice was first removed parallel to the axis of the HIPing can. Specimens were then machined in the plane of this slice. The final surface finish was achieved with p1200 grit SiC paper, to a target thickness of 0.5 mm ±1% (±0.005 mm). While the majority of specimens conformed to this specification, a number of 'over-thinned' specimens (0.485 – 0.495 mm thick) were also tested. These are indicated in the results where included. Post-test microscopy of fracture surfaces in the present study was carried out with a TESCAN FEG SEM.

In accordance with the CEN Workshop Agreement (CWA 15627), a punch radius of 1 mm was used [22]. Testing was carried out using a servo-hydraulic rig with applied loads increasing in 75 N increments from 600 N to 825 N (with an extra 14YWT test at 630 N). These loads were chosen to evaluate the rapid testing capabilities of the SPC approach. All tests were carried out at a temperature of 550 °C, in line with the expected upper operating temperature limit of Eurofer97 [6]. Loading was carried out at a rate of 2.5 N/s, while the time to reach load was excluded from time-to-failure data. Deformation was recorded via a ceramic rod in contact with the underside of the specimen, linked to an extensometer (see item 5 in Figure 1(a)). In accordance with the draft standard, this extension measurement is referred to as 'deflection' (whereas 'displacement' refers to the position of the punch head tip) [24][26]. While the 14YWT was tested under argon, the Eurofer97 was tested in air. To account for this variation, a separate study was carried out by Dawson et al to investigate the influence of environment on SPC testing of Eurofer97 [32]. Interpretation of the Eurofer97 results in Sections 3.2 and 4 are informed by the outcome of this study.

2.1 Force-Stress Conversion Methodologies

As mentioned earlier, SPC can readily provide a qualitative assessment of a material's performance by ranking it against others [21]. However, for a more quantitative evaluation, some means of converting the SPC test load to an equivalent uniaxial stress is needed. What follows is a brief explanation of some existing methodologies, and the rationale behind using the Modified Chakrabarty (MCH) approach [29] in this study.

The central issue is that the stress state within a small punch specimen is a complex multiaxial one that changes throughout the test [23][25]. This makes conversion of an SPC test load to a uniaxial equivalent stress somewhat difficult [23] and has hindered wider use of the technique [29].

However, among the ongoing efforts to standardise SPC are attempts to improve the analysis and interpretation of results [29][26]. The original CEN Workshop Agreement 15627 made use of analysis by Chakrabarty on stretch forming of circular blanks over hemispherical punch heads [22]. This approach ignores bending stresses and describes a biaxial stress state within a membrane stretched over a hemispherical punch [22][33]. The equation derived takes the form:

$$\frac{F}{\sigma} = 2\pi \cdot h \cdot r \cdot \theta_0 \tag{1}$$

Where *F* is the applied load (N), *σ* is the equivalent stress (MPa), *r* is the punch radius (mm), θ_0 is the angle at the contact boundary (radians) and *h* is the disk thickness at the contact boundary (mm) (see Figure 2(a)). The value of *h* can be found from:

$$h = h_0 \left\{\frac{1+\cos\theta_0}{1+\cos\theta}\right\} \tag{2}$$

Where h_0 is the initial disk thickness (mm) and θ is the angle at the clamped boundary (see Figure 2(a)). The relationship between θ and θ_0 is defined as follows:

$$\sin\theta = \frac{r}{R} sin^2\theta_0 \tag{3}$$

Where *R* is the radius of the receiving aperture (mm) (see Figure 2(a)). Chakrabarty also derived an expression for the central displacement of the punch, u_1 (or deflection, as in this case):

$$u_1 = R\sin\theta\, ln\frac{\tan\left(\frac{\theta_0}{2}\right)}{\tan\left(\frac{\theta}{2}\right)} + r(1-\cos\theta_0) \tag{4}$$

From Equations 1-4, *F/σ* can then be plotted as a function of deflection, see Figure 2(b) (solid black line). It can be seen that the equivalent stress varies throughout a test, reaching a minimum at a deflection of approximately 1.4 mm (maximum *F/σ*). This is based on the specific test setup employed in this study (*r* = 1 mm). For the current standard setup (*r* = 1.25 mm), *F/σ* reaches a maximum at a deflection of 1.57 mm [29]. As explained in CWA 15627, regression analysis was then employed to produce a general formula based on the test setup parameters [22]:

$$\Psi = \frac{F}{\sigma} = 3.33 \cdot k_{SP} \cdot R^{-0.2} \cdot r^{1.2} h_0 \tag{5}$$

Where k_{SP} is an SPC test correlation factor introduced to account for the variation in creep ductility between different materials, temperatures and stresses. Taking 1 as the default value for k_{SP}, the general formula provides an estimate of the stress based on the maximum *F/σ* ratio in the Chakrabarty curve. This value is independent of deflection, as illustrated by the dashed black line in Figure 2(b). Since SPC tests may spend much of their duration outside the maximum *F/σ* state, the reliability of this method is highly dependent on the accuracy of k_{SP}. If good correlations with uniaxial data have been established, this should not be an issue. However, in the absence of such data, the reliability of any predicted stress will be limited [29]. Consequently, the new draft standard introduced a fully empirical deflection dependent model [24][26]:

$$\Psi = \frac{F}{\sigma} = 1.9162 \cdot u_{min}^{0.6579} \tag{6}$$

Where u_{min} is the deflection at minimum deflection rate. Although this approach has been shown to reliably estimate equivalent uniaxial creep stresses in SPC tests [29], it applies specifically to the standard test setup (*r* = 1.25 mm) and may therefore be inaccurate in this case (*r* = 1 mm). However, Holmstrom et al have proposed a modified Chakrabarty (MCH) approach that can account for different test setups while retaining deflection dependence [29]. This is based upon the slope of the

Chakrabarty curve at 60% of the deflection at which Ψ reaches its maximum (see Figure 2(b)). The gradient is defined at 60% in order to mimic the curve of the empirical model in the draft standard [29] but will depend on the specific setup employed. The intercept is determined by passing the slope through a fixed point given by:

$$\Psi_{MCH(u_m)} = \frac{F}{\sigma} = (1 + h_0/r) \cdot \Psi_{Cha(u_m)} \quad (7)$$

Where u_m is the deflection at maximum Ψ. This point is based on an estimation of the ultimate tensile strength of ductile materials [29]. Applying the MCH methodology to the setup used in this study (r = 1 mm, R = 2 mm), the following equation was determined for 0.5 mm thick specimens:

$$\Psi_{0.5mm} = 1.0649u_{min} + 0.6630 \quad (8)$$

Since the MCH approach accounts for h_0, additional formulae were derived to incorporate non-standard specimens in the results (in this case, 0.485 mm and 0.49 mm thick):

$$\Psi_{0.485} = 1.0329u_{min} + 0.6223 \quad (9)$$

$$\Psi_{0.49} = 1.0436u_{min} + 0.6357 \quad (10)$$

3. Results

3.1 Microstructure and Microhardness

Figure 3 illustrates the starting microstructures, as imaged via EBSD. The bimodal grain size of the ODS steel required imaging at both high and low magnification, whereas the Eurofer97 could be adequately represented at an intermediate magnification. Figure 3(a) illustrates the Eurofer97 microstructure through Inverse Pole Figure (IPF) colouring of the ferrite phase, with a reference axis perpendicular to the plane of the EBSD map. The original map contained 91.27% successfully indexed points/pixels. To facilitate more reliable grain size analysis, noise in the data was reduced by removing wild spikes and using the nearest neighbours to each zero solution (iterating from eight down to three nearest neighbours). Grain size was determined via post-processing software using the equivalent circular diameter method. A lower limit of three pixels per grain was set and boundaries were defined by a minimum misorientation of 5°. With these parameters, the mean grain diameter of the Eurofer97 was found to be 1.3 µm.

Figure 3(b) illustrates the 14YWT microstructure at low magnification. The black regions indicate areas where the grain structure was too fine to be indexed reliably. Consequently, these were mapped at higher resolution to reveal the finer microstructure, as shown in Figure 3(c). Using the same parameters as above, the mean grain diameter was found to be 4.3 µm at low magnification and 300 nm in the finer regions [30]. From the hardness tests, the Eurofer97 was found to have a Vicker's hardness of 227 HV ±1 (95% confidence limit). However, the hardness value of the 14YWT ODS steel was considerably higher, at 435 HV ±4.

3.2 Small Punch Creep Behaviour

Figure 4 illustrates the time to failure of Eurofer97 and 14YWT as a function of load at 550 °C. Unfortunately, data from specimens conforming to the thickness tolerance of 1% were unavailable for the 14YWT at 750 N. However, it can still be seen that the 14YWT ODS steel outperforms the Eurofer97. The investigation by Dawson et al revealed that testing under argon could increase the

time to failure and deflection at failure of Eurofer97 by up to 30% and 7%, respectively [32]. No significant effect was observed on the minimum deflection rate [32]. To illustrate the potential effect of this on the Eurofer97 data in this study, a correction has been applied in Figure 4. The solid blue line is fitted to the actual (in air) data, while the blue dashed line has been shifted by 30% to reflect the maximum effect of testing in argon. It can be seen that the 14YWT still retains a significant advantage over the Eurofer97. This difference is reflected in the minimum deflection rate, illustrated in Figure 5 as a function of load. Both materials also adhere to the Monkman-Grant relationship between minimum deflection rate and time-to-failure, see Figure 6 [34]. Although the draft standard includes an equation for converting between minimum deflection rate and minimum uniaxial strain rate, this was empirically derived from the standard test set-up (i.e. a punch radius of 1.25 mm) and is therefore inapplicable here (where a punch radius of 1 mm was used) [24][26]. However, the validity of the Monkman-Grant relationship should lend confidence to the predictability of material behaviour.

Representative secondary electron (SE) micrographs of fracture surfaces are presented in Figure 7. Both Eurofer97 and the 14YWT produced 'caps' that separated from the specimens at failure, as is typical of small punch tests of ductile materials [29]. However, it can be seen that the ODS steel also experienced significant radial cracking, suggesting that it has lower ductility than the Eurofer97. This is supported by the lower deflection at failure of 14YWT (Figure 8(a)), which also appears stiffer, in that it exhibits lower deflection under initial loading (Figure 8(b)).

Referring to Figure 8(a), the total deflection (deflection at failure) is shown to be relatively uniform across all loads for Eurofer97 (≈1.6 mm), whereas the total deflection of 14YWT appears to vary linearly with test load, ranging from around 0.8 mm (600 N) to approximately 1.25 mm (825 N). The cause of this load dependence is unclear. One possibility is that a change of deformation mode is occurring. Given the relatively short duration of these SPC tests (i.e. relatively high load), it may be that they straddle the boundary between diffusional and dislocation based deformation processes. At high loads, dislocation processes are expected to dominate [35], giving rise to a more ductile, transgranular fracture, whereas at lower loads, a more brittle, intergranular fracture is expected [36][37].

4. Discussion

The superior time-to-failure data of the 14YWT relative to Eurofer97 is not unexpected in light of the oxide dispersion strengthening [7]. This strengthening is also reflected in the much higher room temperature hardness of the 14YWT (435 HV vs 227 HV), although the thermal stability of oxide particles is less pertinent at such temperatures [8][9]. Additional hardening mechanisms may also contribute to the higher strength of the 14YWT e.g. the fine grained regions of the microstructure shown in Figure 3(c). However, as Figures 7 and 8 illustrate, the higher strength and time-to-failure performance may come at the expense of ductility. Again, this is not unexpected as strength and ductility are often inversely correlated [38]. However, that isn't to say further microstructural optimisation isn't possible. The bimodal grain size may be one aspect of the microstructure that could improve ductility through careful modification [39][40].

Thus far, the performance of Eurofer97 and 14YWT have only been compared in relative terms. Therefore, using the MCH approach described in Section 2.1, the test loads were converted to estimated uniaxial equivalent stresses, and the revised data is presented in Figure 9(a). While the 14YWT appears to retain its superior performance relative to Eurofer97, a significant amount of

scatter is introduced, and the expected relationship between stress and time-to-failure breaks down. This raises doubts over the accuracy of the 14YWT estimated stress values. While the Eurofer97 data also exhibited an increase in scatter, the trend is still reasonable. The irregular effect of the force-stress conversion process on the 14YWT may be related to its relatively low ductility. As pointed out in CWA 15627, the Chakrabarty analysis is not valid at low strains, as the bending moment is ignored and F/σ approaches zero (i.e. membrane stresses tend to infinity) [22]. As Figure 8 illustrated, the 14YWT failed at significantly lower deflections than the Eurofer97, possibly compromising the accuracy of the stress estimates.

Another potential issue is the determination of u_{min}. As illustrated in Figure 10, the deflection rate of Eurofer97 reaches a more obvious minima than 14YWT, and may therefore provide a more consistent deflection from which to estimate equivalent stress. The deflection rate of 14YWT 'levels off' more clearly, but this may actually introduce more scatter in u_{min}, as smaller variations in the deflection rate will shift u_{min} more dramatically. In addition, issues with data acquisition and smoothing can further complicate the determination of u_{min}. These problems were encountered in the development of MCH, and led to suggestions that a more consistent option might be the use of deflection at $1/2t_r$ (half rupture time) [29]. To assess the effect of such a methodology, the data was re-evaluated based on $1/2t_r$, and is presented in Figure 9(b). The Eurofer97 data appears almost unchanged. However, although the 14YWT scatter may have reduced slightly, there is still no reliable trend.

The deflection dependence of the MCH approach is intended to compensate for the variation in equivalent stress that occurs throughout an SPC test. Within the deflection range of most tests, Chakrabarty's analysis shows the membrane stress falling as deflection rises, see Figure 2(b). Lower load tests (which spend longer at lower deflections) may therefore be subjected to higher equivalent stress than expected, which the MCH model adjusts for. However, if there is overcompensation, this might lead to overestimation of the stresses in lower load (i.e. longer duration) tests and vice versa, thus 'flattening' the trendline in stress-time to failure data. As illustrated in Figure 8, the 14YWT exhibited significantly more variation in total deflection (deflection at failure) than the Eurofer97. Consequently, there was much greater variation in the deflection values used to estimate equivalent stresses. This behaviour might be responsible for the erratic force-stress conversion results of the 14YWT, and may render it unsuitable for analysis by MCH. However, under equivalent loads, ODS 14YWT has nevertheless demonstrated significant promise as a high temperature, creep resistant alloy, relative to Eurofer97.

5. Conclusions

This study assessed the small punch creep properties of Eurofer97 and 14YWT ODS steel at 550 °C. The 14YWT demonstrated superior time-to-failure and significantly lower rates of deformation. However, it also suffered reduced ductility and exhibited a mixed mode failure. The Modified Chakrabarty (MCH) approach was employed to estimate equivalent uniaxial creep stresses. While the conversion was relatively smooth for Eurofer97, it introduced a significant amount of scatter in the 14YWT data. Since the MCH method assumes membrane stretching behaviour, the low ductility of 14YWT may have been responsible for the erratic force-stress conversion results. Further work is needed to identify the limits of existing models and, where necessary, develop models for materials with reduced ductility. These issues made accurate estimation of the 14YWT performance difficult, but did not undermine the conclusion that it possessed superior creep resistance, in terms of both time-to-failure and dimensional stability (a key concern of designers). However, given the relatively

high load (short duration) regime of the testing, care should be exercised in extrapolating from this to longer timescales, as the dominant deformation mode is likely to change.

Acknowledgements

This work has been funded by the RCUK Energy Programme [grant number EP/T012250/1. To obtain further information on the data and models underlying this paper please contact PublicationsManager@ukaea.uk

This research made use of the UKAEA's Materials Research Facility, which has been funded by and is part of the UK's National Nuclear User Facility and Henry Royce Institute for Advanced Materials.

The authors also wish to thank the Karlsruhe Institute of Technology for supply of the Eurofer97 rolled plate.

References

[1] I. T. Chapman and A. W. Morris, "UKAEA capabilities to address the challenges on the path to delivering fusion power," *Philos. Trans. R. Soc. A Math. Phys. Eng. Sci.*, vol. 377, no. 2141, 2019.

[2] E. Surrey, "Engineering challenges for accelerated fusion demonstrators," *Philos. Trans. R. Soc. A Math. Phys. Eng. Sci.*, vol. 377, no. 2141, 2019.

[3] D. Stork and S. J. Zinkle, "Introduction to the special issue on the technical status of materials for a fusion reactor," *IOP*, vol. 57, 2017.

[4] D. Stork *et al.*, "Materials R&D for a timely DEMO: Key findings and recommendations of the EU Roadmap Materials Assessment Group," *Fusion Eng. Des.*, vol. 89, no. 7–8, pp. 1586–1594, 2014.

[5] D. Stork *et al.*, "Assessment of the EU R&D Programme on DEMO Structural and High-Heat Flux Materials." EUROfusion, 2012.

[6] H. Tanigawa *et al.*, "Development of benchmark reduced activation ferritic/martensitic steels for fusion energy applications," *Nucl. Fusion*, vol. 57, no. 9, 2017.

[7] S. J. Zinkle *et al.*, "Development of next generation tempered and ODS reduced activation ferritic/martensitic steels for fusion energy applications," *Nucl. Fusion*, vol. 57, no. 9, 2017.

[8] M. J. Alinger, G. R. Odette, and D. T. Hoelzer, "The development and stability of Y-Ti-O nanoclusters in mechanically alloyed Fe-Cr based ferritic alloys," *J. Nucl. Mater.*, vol. 329–333, no. 1-3 PART A, pp. 382–386, 2004.

[9] S. Y. Zhong *et al.*, "Study of the thermal stability of nanoparticle distributions in an oxide dispersion strengthened (ODS) ferritic alloys," *J. Nucl. Mater.*, vol. 428, no. 1–3, pp. 154–159, 2012.

[10] D. Stork *et al.*, "Developing structural, high-heat flux and plasma facing materials for a near-term DEMO fusion power plant: The EU assessment," *J. Nucl. Mater.*, vol. 455, no. 1–3, pp. 277–291, 2014.

[11] A. Ibarra *et al.*, “The IFMIF-DONES project: Preliminary engineering design,” *Nucl. Fusion*, vol. 58, no. 10, 2018.

[12] A. Ibarra, “IFMIF-DONES progress and future plans,” pp. 1–35, 2019.

[13] F. Arbeiter *et al.*, “Planned material irradiation capabilities of IFMIF-DONES,” *Nucl. Mater. Energy*, vol. 16, no. December 2017, pp. 245–248, 2018.

[14] J. Averhals *et al.*, “Design description and validation results for the IFMIF High Flux Test Module as outcome of the EVEDA phase,” *Nucl. Mater. Energy*, vol. 9, pp. 59–65, 2016.

[15] T. Yokomine, S. Ebara, and A. Shimizu, “Thermo-hydraulic design of high flux test module for ifmif-eveda in Japan,” *Fusion Sci. Technol.*, vol. 56, no. 1, pp. 267–272, 2009.

[16] P. Jung, A. Hishinuma, G. E. Lucas, and H. Ullmaier, “Recommendation of miniaturized techniques for mechanical testing of fusion materials in an intense neutron source,” *J. Nucl. Mater.*, vol. 232, no. 2–3, pp. 186–205, 1996.

[17] B. Giannone *et al.*, “IFMIF Comprehensive Design Report,” p. 138, 2004.

[18] J. Knaster *et al.*, “Overview of the IFMIF / EVEDA project,” 2017.

[19] D. Stork *et al.*, “Towards a programme of testing and qualification for structural and plasma-facing materials in ‘fusion neutron’ environments,” *Nucl. Fusion*, vol. 57, no. 9, 2017.

[20] M. Kapusňák, J. Petzová, M. Březina, and M. Adamech, “Interim results of the reactor pressure vessel materials evaluation within the framework of the implemented Advanced Surveillance Specimen Programme,” in *Proceedings of the 5th International Small Sample Test Techniques Conference*, 2018, pp. 58–66.

[21] R. J. Lancaster and P. J. Spencer, “Small Punch Creep,” in *Intech*, 2017.

[22] CEN, “CWA 15627: Small Punch Test Method for Metallic Materials.” CEN, Brussels, 2007.

[23] M. Bruchhausen *et al.*, “Recent developments in small punch testing: Tensile properties and DBTT,” *Theor. Appl. Fract. Mech.*, vol. 86, pp. 2–10, 2016.

[24] CEN Workshop Agreement, “Small Punch Test Method for Metallic Materials,” *Small Punch Test Method Met. Mater.*, 2006.

[25] A. Janča, J. Siegl, and P. Haušild, “Small punch test evaluation methods for material characterisation,” *J. Nucl. Mater.*, vol. 481, pp. 201–213, 2016.

[26] M. Bruchhausen *et al.*, “European standard on small punch testing of metallic materials,” in *Proceedings of the 5th International Small Sample Test Techniques Conference*, 2018, pp. 1–14.

[27] R. Kopriva, M. Brumovsky, and P. Petelova, “Current status of the small punch test standardization within the ASTM,” in *Proceedings of the 5th International Small Sample Test Techniques Conference*, 2018, pp. 26–30.

[28] A. Morris, B. Cacciapuoti, and W. Sun, “The role of small specimen creep testing within a life assessment framework for high temperature power plant,” *Int. Mater. Rev.*, vol. 63, no. 2, pp. 102–137, 2018.

[29] S. Holmström *et al.*, “Creep strength and minimum strain rate estimation from Small Punch Creep tests,” *Mater. Sci. Eng. A*, vol. 731, no. April, pp. 161–172, 2018.

[30] M. J. Gorley, “Powder processing of oxide dispersion strengthened alloys for nuclear

applications," 2014.

[31] M. D. Richardson, S. Connolly, M. Gorley, B. P. Wynne, and E. Surrey, "Influence of surface finish on small punch testing of 9Cr Eurofer-97 steel," *ASTM J. Test. Eval.*, vol. 48, no. 2, 2020.

[32] H. Dawson, M. Richardson, M. Gorley, and S. E, "The effect of testing environment on small punch creep," in *Proceedings of the 5th International Small Sample Test Techniques Conference*, 2018, pp. 359–369.

[33] J. Chakrabarty, "A theory of stretch forming over hemispherical punch heads," *Int. J. Mech. Sci.*, vol. 2, no. 4, pp. 315–325, 1970.

[34] F. C. Monkman and N. J. Grant, "An Empirical Relationship Between Rupture Life and Minimum Creep Rate in Creep-Rupture Tests," in *ASTM Proceedings 1956*, 1956, pp. 593–620.

[35] N. E. Dowling, *Mechanical Behavior of Materials*, 4th ed. Harlow: Pearson, 2013.

[36] G. S. Deshmukh, M. L. Prasad, D. R. Peshwe, J. Ganesh Kumar, M. D. Mathew, and G. Amarendra, "Creep Properties Assessment of P92 Steel by Small Punch Creep Tests," *Trans. Indian Inst. Met.*, vol. 69, pp. 907–915, 2016.

[37] K. Maruyama, "Fracture mechanism map and fundamental aspects of creep fracture," in *Creep-Resistant Steels*, F. Abe, K. Torstern-Ulf, and R. Viswanathan, Eds. Cambridge: Woodhead Publishing Ltd., 2008, pp. 350–364.

[38] Y. Wei *et al.*, "Evading the strength-ductility trade-off dilemma in steel through gradient hierarchical nanotwins," *Nat. Commun.*, vol. 5, 2014.

[39] A. P. Gulyaev and L. N. Serebrennikov, "Effect of differences in grain size on the mechanical properties of steel 18Kh2N4MA," *Met. Sci. Heat Treat.*, vol. 19, pp. 253–256, 1977.

[40] Z. Dapeng, L. Yong, L. Feng, W. Yuren, Z. Liujiea, and D. Yuhai, "ODS ferritic steel engineered with bimodal grain size for high strength and ductility," *Mater. Lett.*, vol. 65, no. 11, pp. 1672–1674, 2011.

Table 1: Composition of 9Cr Eurofer97 plate and 14Cr ODS steel (14YWT) (wt%)

Alloy	Product Form	Cr	W	Si	Mn	Ti	O	C	Y	Fe
Eurofer97	Plate	8.95	1.06	0.031	0.55	0.001	0.0007	0.11	-	Bal.
14YWT	HIP	13.34	2.81	-	0.38	0.22	0.23	0.08	0.19	Bal.

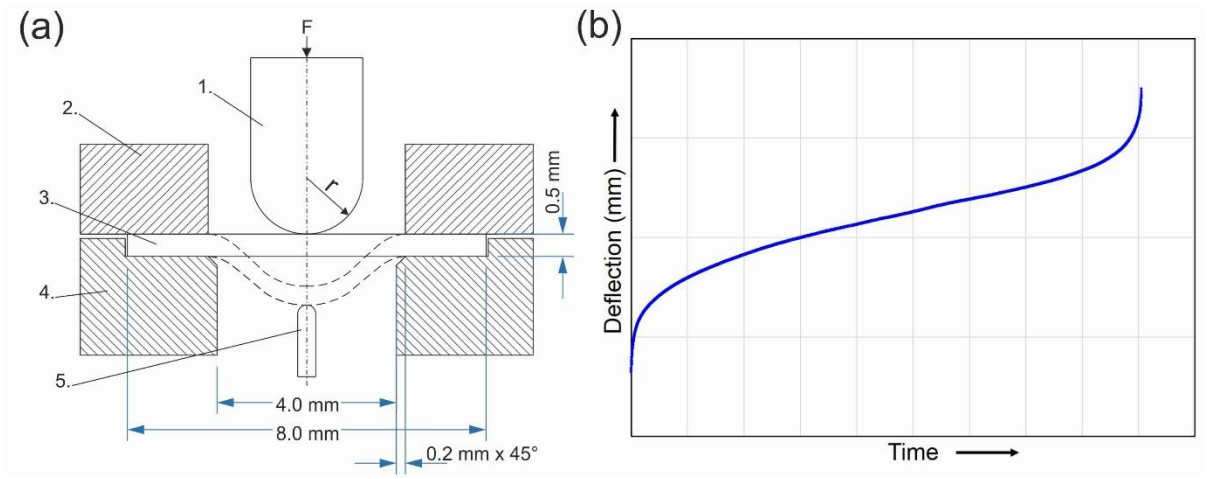

Figure 1: (a) Small Punch Creep (SPC) test setup conforming to CWA 15627 [22]; (1) Punch Head, (2) Clamping die, (3) Specimen, (4) Receiving Die, (5) Extensometer Rod, (b) illustrative small punch creep curve.

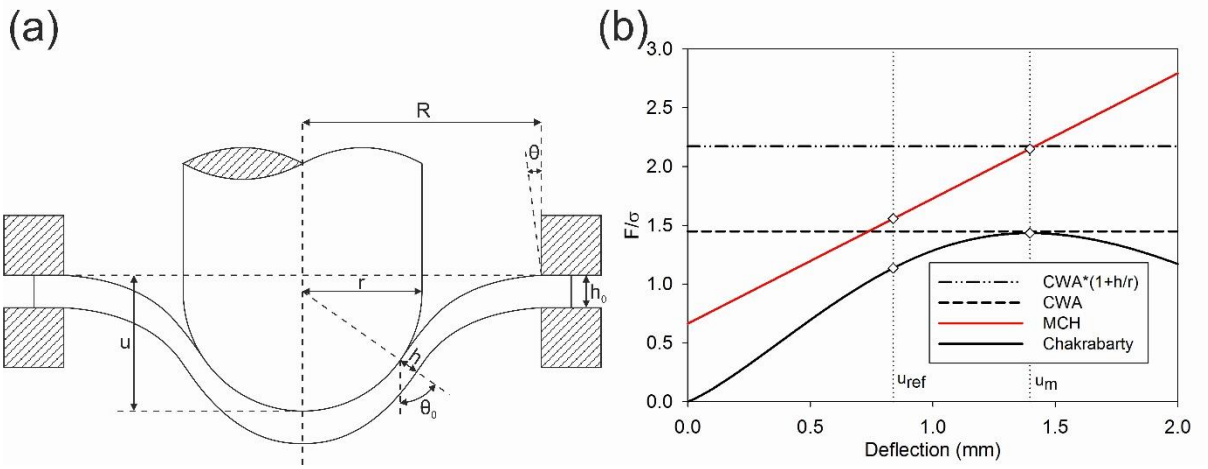

Figure 2: (a) relevant parameters required for Chakrabarty's membrane stretching model and (b) various force-stress conversion methodologies, including the original Chakrabarty approach [22], fitted equation from the CEN Workshop Agreement 15627 (CWA) [22], a modified CWA approach (CWA*(1+h_0/R)) [29] and the Modified Chakrabarty (MCH) method adopted in this paper [29].

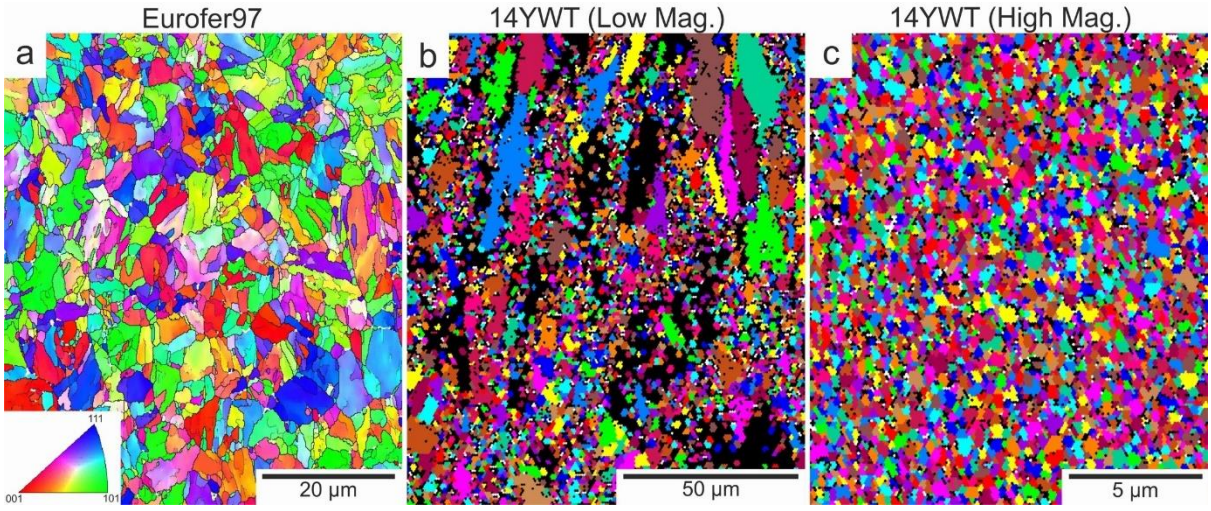

Figure 3: EBSD maps of as-received microstructures, illustrating (a) Eurofer97 plate under Inverse Pole Figure (IPF) colouring and (b)-(c) the bimodal microstructure of 14YWT ODS steel under unique grain colouring [30]. Reference axis for (a) is perpendicular to the plane of the map.

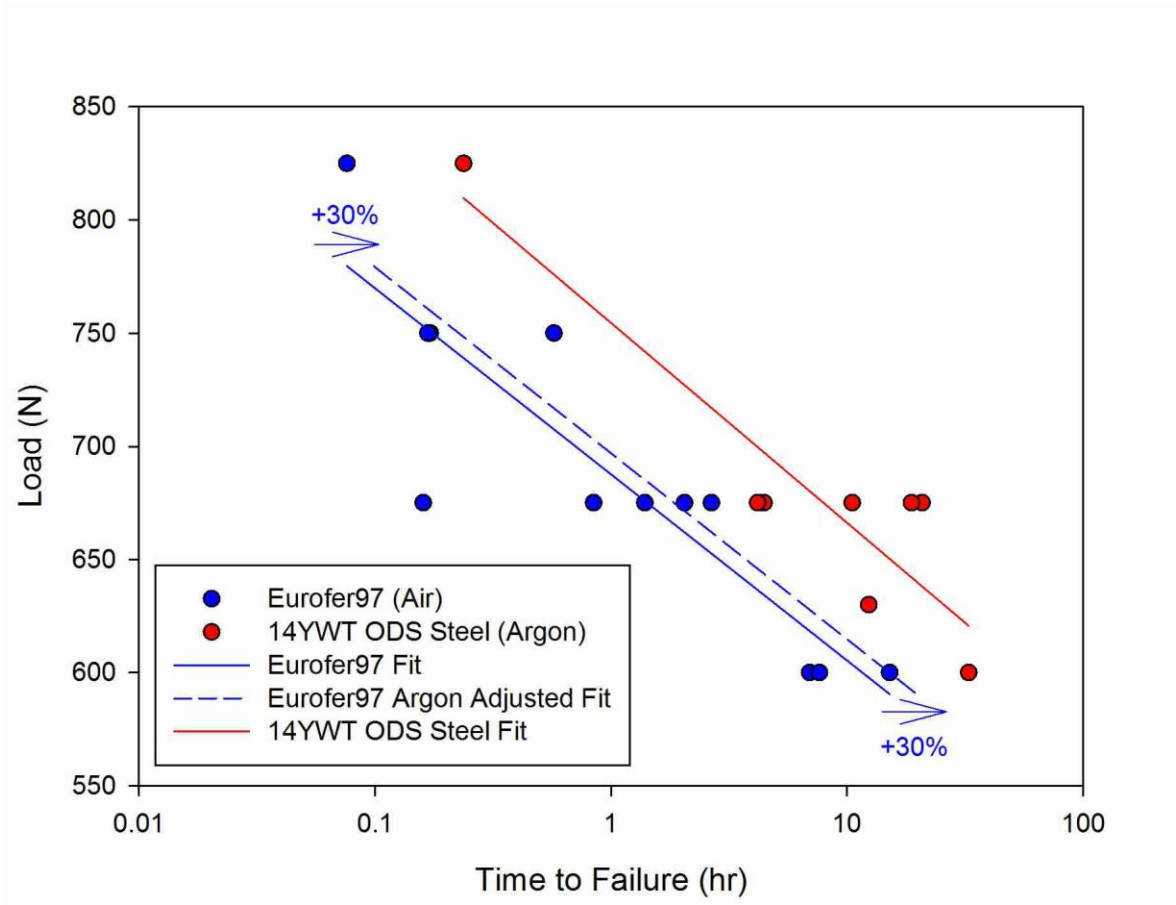

Figure 4: Small Punch Load-Time to failure comparison of Eurofer97 and 14YWT ODS steel at 550 °C, including adjusted Eurofer97 curve to account for differing test environments [32] (Eurofer97 in air, 14YWT ODS steel under argon).

HALF WIDTH VERSION?

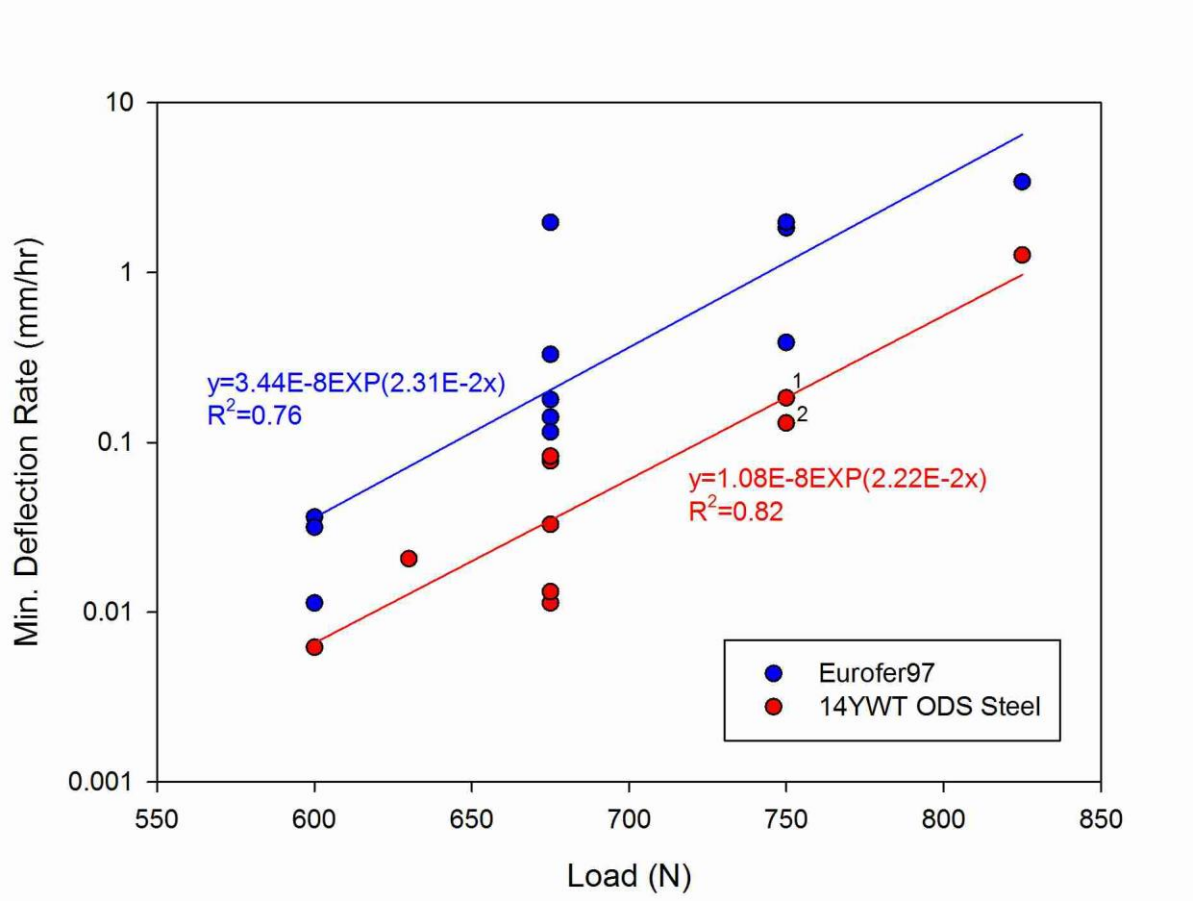

Figure 5: Minimum deflection rate of Eurofer97 and 14YWT ODS steel as a function of load, during small punch creep testing at 550 °C. Numbered specimens are outside specification: 1 (0.485 mm thick), 2 (0.49 mm thick).

HALF WIDTH VERSION?

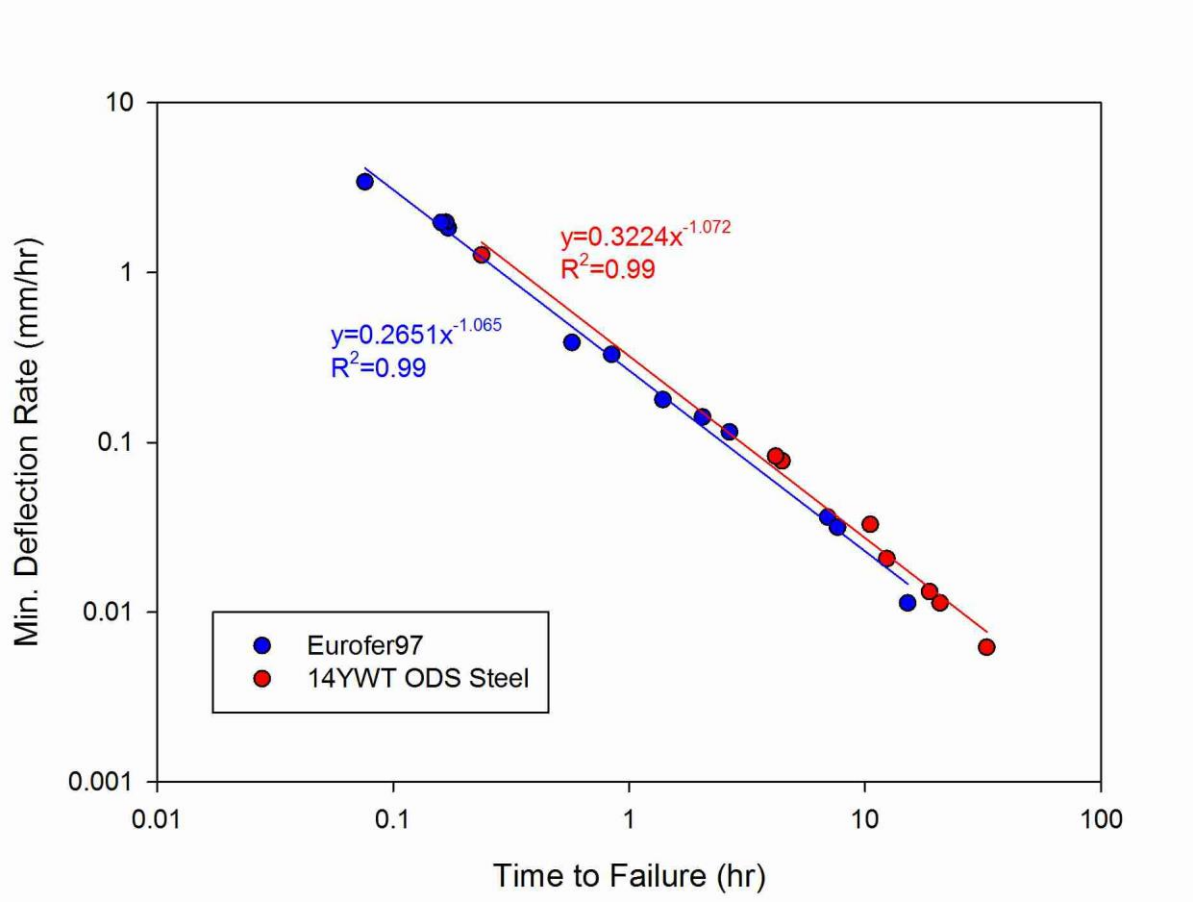

Figure 6: Minimum deflection rate vs time to failure of Eurofer97 and 14YWT ODS Steel at 550 °C, illustrating the Monkman-Grant relationship.

HALF WIDTH VERSION?

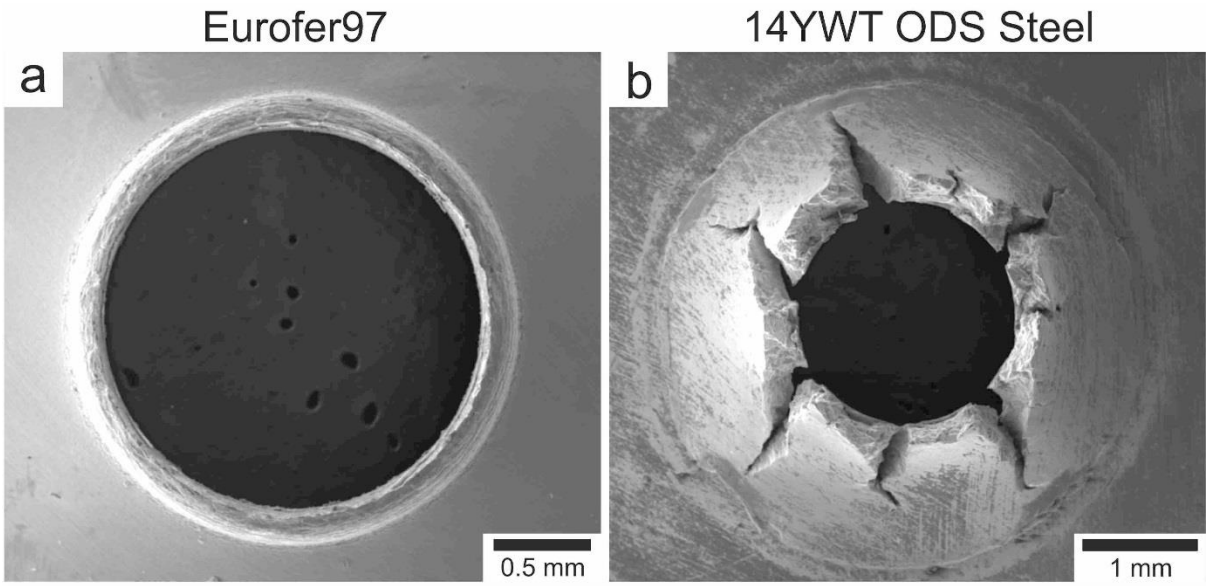

Figure 7: SE micrographs of small punch creep specimens tested at 550 °C.

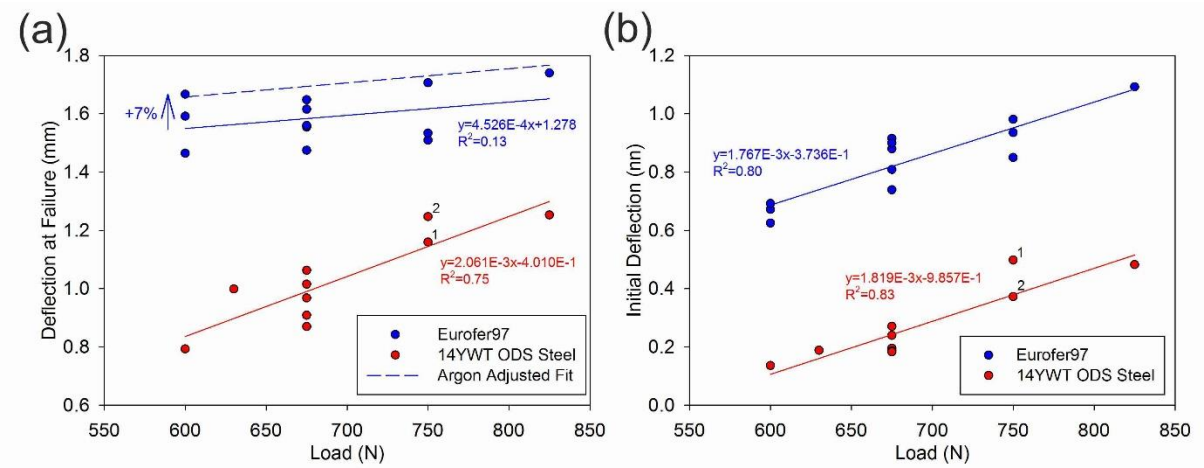

Figure 8: Variation in deflection throughout small punch creep testing of Eurofer97 and 14YWT ODS steel at 550 °C, illustrating (a) deflection at failure (total test deflection), and (b) initial loading induced deflection (time independent deformation). Numbered specimens are outside specification: 1 (0.485 mm thick), 2 (0.49 mm thick) (fitted lines incorporate these data points). Eurofer97 equation applies to unadjusted (in air) data.

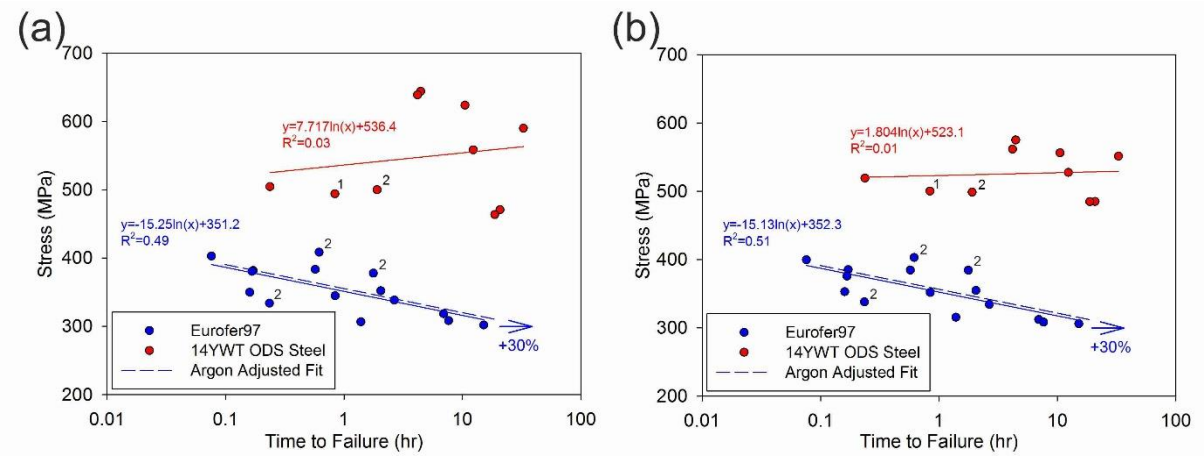

Figure 9: Estimated equivalent uniaxial stress vs time to failure comparison of Eurofer97 and 14YWT ODS steel at 550 °C. Force-stress conversion based on (a) deflection at minimum deflection rate, and (b) deflection at half rupture time. Numbered specimens are outside specification (including additional Eurofer97 data): 1 (0.485 mm thick), 2 (0.49 mm thick) (fitted lines incorporate these data points). Eurofer97 equations apply to unadjusted (in air) data.

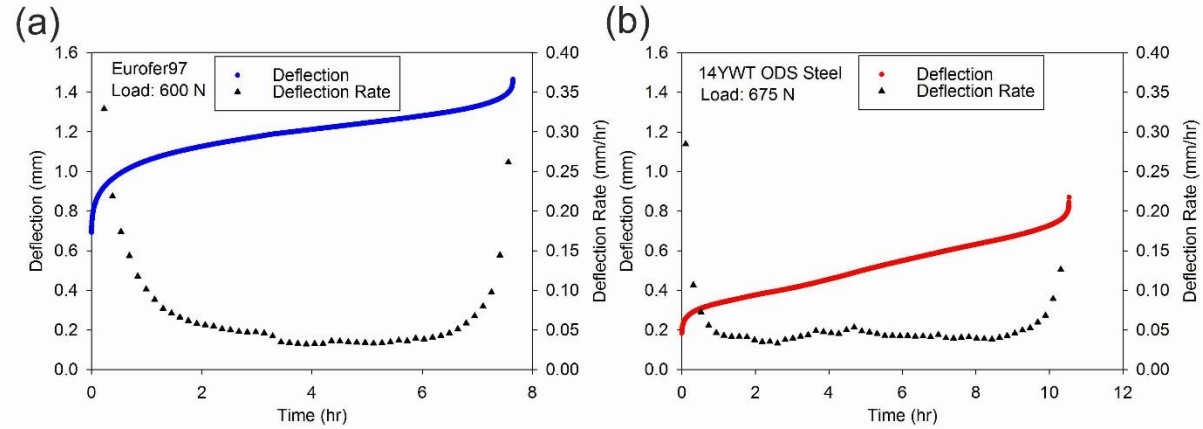

Figure 10: Representative deflection and deflection rate curves of Eurofer97 and 14YWT ODS steel at 550°C under (a) 600 N and (b) 675 N.